Dual-frequency sheath oscillations and consequences on the ion and electron transport in dielectric barrier discharges at atmospheric pressure

Raphaël Robert, Gerjan Hagelaar, Nader Sadeghi, Luc Stafford, Françoise Massines

DUAL-FREQUENCY SHEATH OSCILLATIONS AND CONSEQUENCES ON THE ION AND ELECTRON TRANSPORT IN DIELECTRIC BARRIER DISCHARGES AT ATMOSPHERIC PRESSURE

Raphaël Robert[1,2], Gerjan Hagelaar[3], Nader Sadeghi[4], Luc Stafford[2], Françoise Massines[1]

[1]Laboratoire Procédés Matériaux et Énergie Solaire (PROMES, CNRS, UPR 8521), Rambla de la thermodynamique, 66100 Perpignan, France

[2]Département de physique, Université de Montréal, 1375 ave. Thérèse-Lavoie-Roux, Montréal, Québec, H2V 0B3, Canada

[3]Laboratoire Plasma et Conversion d'Énergie (LAPLACE, CNRS, UMR5213), 118 Route de Narbonne, 31077 Toulouse, France

[4]Laboratoire Interdisciplinaire de Physique (LIPhy CNRS, UMR 5588), Université de Grenoble-Alpes, Grenoble, France

ABSTRACT

Current-voltage characteristics, space- and time-resolved optical emission spectroscopy, and 1D fluid modeling are used to examine the effect of dual-frequency sheath oscillations on the ion and electron transport in dielectric barrier discharges (DBDs) sustained by a combination of low-frequency (LF, 50 kHz, 650 V) and radiofrequency (RF, 5.3 MHz, 195 V) voltages, and exhibiting the α–to–γ mode transition. On one hand, when polarities of the LF and RF voltages are opposite, an electric field near the LF cathode (due to LF cathode sheath) drives the secondary electrons to the plasma bulk and an opposite electric field between the sheath edge and the LF anode attracts the electrons towards the LF cathode (to maintain quasi-neutrality in the plasma bulk). At the sheath edge, electrons become trapped and ions drift towards the cathode and the anode simultaneously according to their position in the gap. On the other hand, when the RF voltage has the same polarity as the LF voltage, the total applied voltage increases and this yields to enhanced production of electrons and ions in the sheath. To maintain quasi neutrality in the bulk, the electric field along the gap exhibits the same polarity as the one in the sheath, allowing electrons created in the sheath to be evacuated towards the LF anode. The behavior of the LF cathode is therefore controlled by the LF sheath, and thus by the LF voltage amplitude, while the behavior in the bulk and at the anode alternates on the time scale of the RF voltage.

1. Introduction

Over the last 50 years, various configurations leading to stable and diffuse dielectric barrier discharges (DBDs) at atmospheric pressure have been established [1]–[5]. Most available studies have been conducted at frequencies of the applied voltage less than 250 kHz, resulting in pulsed discharges whose nature varies depending on the so-called memory effect in which energetic species can be carried from one discharge to the next [6]–[9]. This specific behavior is not observed in the radio frequency (RF) range, wherein the discharge is rather continuous, and the time-averaged number density of ions and electrons, partially trapped in the plasma bulk, is much higher than at low frequency (LF) [10], [11]. Moreover, in the RF range, the breakdown voltage is lower than at LF [12], [13], and only a small portion of the applied voltage falls across the solid dielectrics due to rapid voltage oscillations [14]. As a result, the discharge is no longer dominated by the effects of the dielectrics, and the ionization degree is governed by the amplitude of the instantaneous applied voltage [15]–[17]. When the power absorbed or dissipated by the plasma electrons is increased, a transition from the RF-α to the RF-γ mode can be reached [18]–[23]. This α – γ transition induces a significant flux of ions to the cathode and thus the emission of a large number of secondary electrons; hence, there is a strong electron multiplication in the sheath. In this γ mode, a solid dielectric placed on the metallic electrodes is necessary to avoid discharge localization and to improve the discharge stability [24].

More recently, dual-frequency DBDs (DF-DBDs) have emerged as stable, high power DBDs that can be easily implemented in plane-to-plane or jet configurations [18], [25]–[27]. In DF-DBDs, one electrode is powered by LF voltage (< 250 kHz), whereas the other one is powered by RF voltage (for example, 5 MHz or 13.56 MHz). The two voltage signals are typically synchronized, and the power supplies have a common ground. So far, many studies have been conducted on DF-DBDs in Ar-based gas mixtures, and various configurations have been examined [19], [23], [25], [26], [28], [29]. In such conditions, it was found that

secondary electron emission from the cathode does not only rely on positive ions and Ar metastables irradiation: the VUV photons resulting from the spontaneous de-excitation of the Ar_2^* excimer produced by fast conversion of Ar(1s) metastable states also contribute to secondary electron emission, and thus to electron multiplication in the sheath [30].

In DF-DBDs, two modes can be reached, α or α – γ modes. The α regime in DF-DBDs exhibit the same behavior as in single-frequency RF DBDs characterized by ohmic heating of plasma electrons in the bulk where the electron temperature is quite low [17], [31], [32]. However, the power absorbed or dissipated by the plasma electrons in α DF-DBDs is lower than that of a RF DBD generated at the same RF voltage amplitude [23]. Such variation may be attributed to the effect of the LF voltage in inducing ion loss at the walls, which in turn decreases the plasma density [23]. As for the α – γ DF-DBDs, they alternate between α and γ mode at the LF time scale. γ mode is observed when the electric field established in the sheath is high enough to induce a self-sustained discharge in the LF cathode sheath [23]. Specifically, the high-electric field condition accelerates the flux of secondary electrons across the collisional sheath, thereby promoting electron multiplication and increasing the production of positive ions, VUV photons, and additional secondary electrons in the sheath [30]. The gamma mode is initiated over several RF cycles, each time the LF voltages approaches its maximum (i.e. twice per LF period). In such conditions, since the ions only weakly "see" the RF modulations due to their larger mass than the electrons, they flow continuously towards the cathode. This results in continuous secondary electron emission, which reduces the voltage applied to the gas and thus increases the voltage across the dielectrics. Since the duration of the γ behavior in DF-DBDs is limited by the decrease in gas voltage [14], as in the case of a LF discharge, this mode can last for a few microseconds in the LF cycle (about 10 %), such the α – γ DF-DBD is in α regime most of the time (about 90 %) [23]. Compared to the α mode, this γ regime is characterized by higher time-

averaged electron number densities (N_e) and temperatures (T_e) due to increased electron multiplication and enhanced electric field in the cathode fall, respectively [14].

Several studies have been conducted on α and α – γ DF-DBDs operated in Ar-based gas mixtures. Specifically, the α and α – γ modes were compared, and the effects of LF voltage amplitude [23], [26], [29], [31], RF voltage amplitude [14], [26], [27], phase between the two voltage signals [33]–[35], and number of harmonics on a fundamental frequency [36], [37] were examined. However, to the best of knowledge, the influence of RF polarity oscillations on the transport properties of charged species in α – γ DF-DBDs has not been reported. In this work, a combination of experimental measurements and simulations is used to examine the effect of dual-frequency sheath oscillations on the ion and electron transport in an α – γ DF-DBD generated in Ar-NH_3 gas mixtures at atmospheric pressure. For this purpose, the current-voltage characteristics are measured, and the space- and time-resolved optical emission intensities from Ar(2p-1s) lines and bremsstrahlung continuum emission intensities are also recorded. Electrical and optical measurements are further analyzed in combination with the predictions of a 1D fluid model of Ar-based DBDs described and validated in a previous work [30].

2. Experimental set-up and diagnostics

A full description of the plane-to-plane DBD system used in this study is provided in [14], [30]. Briefly, the setup consists of two metallic electrodes (1 x 5 cm^2) covered with a 1-mm-thick layer of alumina dielectric (7 x 7 cm^2) and mounted in plane-to-plane configuration at 2 mm gap distance. The DBD cell is housed in a plasma chamber that is first vacuumed down to 1 mTorr and then filled with Ar + 200 ppm of NH_3 at 3 standard liters per minute up to 760 Torr. A needle valve between the chamber and the pumping system

allows maintaining the atmospheric pressure condition. The upper electrode is powered by a 50 kHz LF generator, whereas the lower one is connected to a 5.3 MHz RF generator. The LF and RF voltage amplitudes are set to 650 V (50 V above the breakdown voltage of the 50 kHz LF discharge) and 195 V (50 V above the breakdown voltage of the 5.3 MHz RF discharge), respectively. Both waveforms are generated using the same generator (Keysight 33500B series) to ensure adequate synchronization and common ground. The generator is connected to an audio amplifier (Crest CC4000) linked to a bridged resistor and a step-up voltage transformer (Boige & Vignal) for the LF contribution and a broadband power amplifier (PRANA GN500) and a homemade transformer for the RF part (REF). Unlike commercial RF generators, here, the impedance of the whole transmission line cannot be adjusted to reduce the reflected power; therefore, to maximize the transmitted power, a possible way is to slightly change the RF frequency [rajouter la ref 10 ici] around the nominal 5 MHz value. Over the range of experimental conditions investigated, 5.3 MHz is chosen. Current-voltage characteristics are recorded using a current probe (Lilco 13W5000) and two high-voltage probes (Tektronix P6015A) set on electrodes, and they are visualized on an oscilloscope (Tektronix MSO56).

Space- and time-resolved optical emission spectra of the DF-DBD are recorded using the method described in a previous study [14]. This optical system comprises a lens and a set of 3 mirrors that are used to project the plasma image of the DBD gap on the entrance slit of a Czerny–Turner monochromator (Jobin-Yvon, 66 cm focal length, 1200 groves/mm grating). Herein, the magnification factor and slit opening were fixed at 1.95x and 150 µm, respectively, resulting in a spatial resolution of 77 µm across the 2 mm DBD gap. The system further relies on a photomultiplier tube module (Hamamatsu H10721-20) operated in photon counting mode and a multichannel photon counter (MSC6A2T8 Fast Comtec), triggered by the LF power supply. Herein, the parameters of the photon counter were set to achieve 6.4 ns time resolution.

3. Experimental results

3.1 Current-voltage characteristics of the α – γ DF-DBDs

Figure 1 (a) and Figure 1 (b) present the current-voltage characteristic of the Ar-based DBD recorded over a single LF cycle. As shown in Figure 1 (a), the current is strongly modulated by the applied RF voltage. In addition, Figure 1 (a) reveals that the current averaged over the RF cycle displays an offset, with either a positive or negative value depending on the amplitude of the LF voltage. These observations remain valid throughout the LF cycle, except around LF current inversion (*i.e.*, at 5.5 and 15.5 µs), when the LF voltage applied to the gas changes polarity (recall that in DBDs operated in a glow regime, the LF voltage applied to the gas (not shown in Figure 1 (b)) does not correspond to the LF voltage applied to the electrodes (shown in Figure 1 (b)) due to the presence of charges on the dielectric surfaces [38]). Moreover, in line with previous studies of RF discharges [39], [40], the currents maxima are delayed by about 48 ns (about a quarter of the RF period, 188 ns at 5.3 MHz) relative to the applied RF voltage. Figure 1 (a) further shows that the current amplitude is enhanced between 1.1 and 2.7 µs, as well as between 11.1 and 12.7 µs. In these time intervals, a drastic increase in the LF current amplitude (averaged over the time scale of the RF cycle) is observed, suggesting that the DBD is in the γ mode. As described above, this regime is characterized by a strong ionization in the cathode sheath such that the discharge becomes self-sustained in this region [30]. Beyond 2.7 µs, the amplitude of RF modulation (and thus the amplitude of the LF current) decreases, and the discharge transits from γ mode to the RF-α mode. This transition is due to the strong increase of the current in γ mode leading to the high charging of dielectric plates. In a dielectric barrier discharge, the applied voltage is distributed between the gas gap and the dielectrics; when dielectrics become charged, the LF voltage across dielectrics increases and thus, the LF voltage applied to the gas decreases [14]. This behavior results in the extinction of a single frequency LF glow discharge. Here,

due to the RF voltage component always turning on the discharge, a transition from γ to α mode is seen.

In Section 3.2, optical diagnostics are shown between 0.5 and 3 µs during which the discharge transits to the γ mode. Then, in Section 3.3, simulations are presented in the same time interval for the α – γ DF-DBD. Finally, in Section 3.4, a comparative simulation study is done for the α DF-DBD.

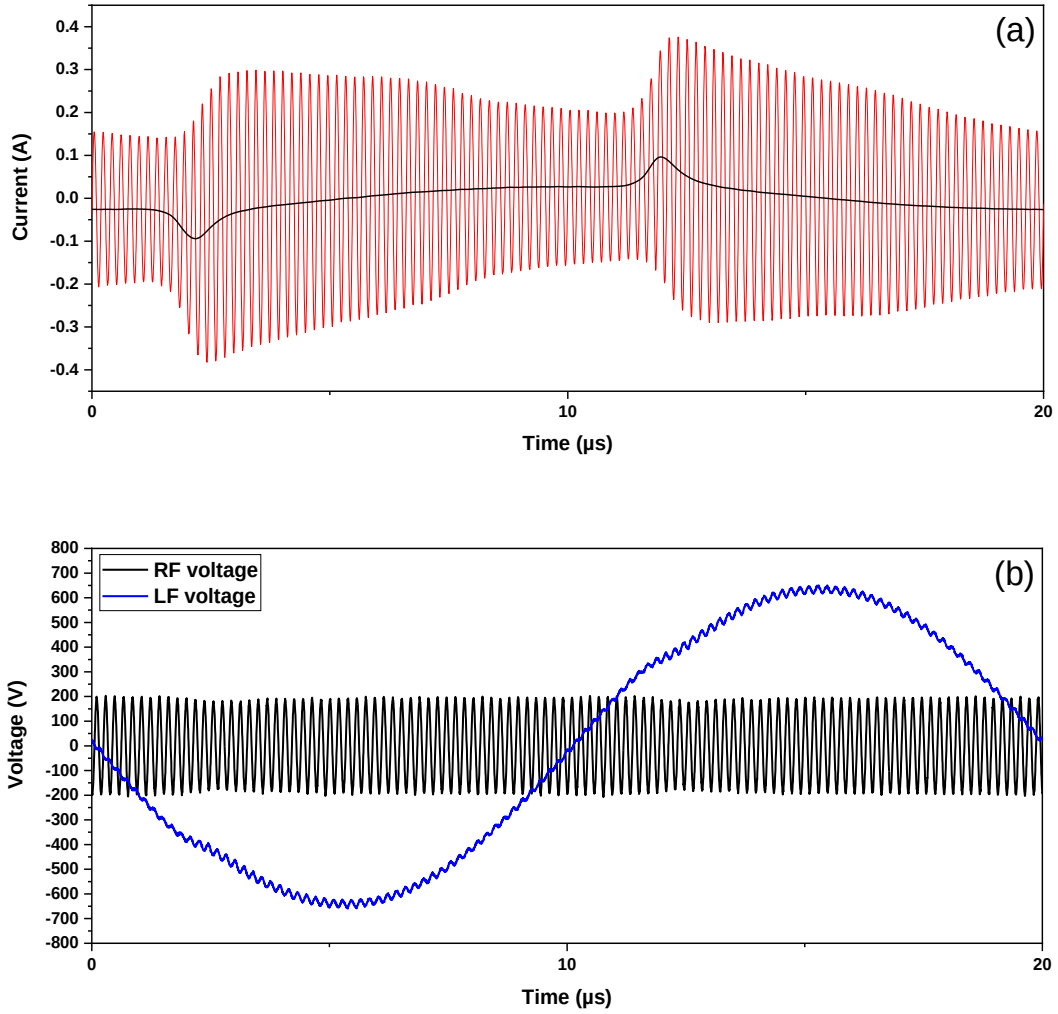

Figure 1. (a) Temporal evolution of the measured current (in red) in the Ar-based DBD for which the upper electrode is powered by a 50 kHz LF generator (period of 20 µs), whereas the lower one is connected to a 5.3 MHz RF generator (period of 188 ns). Here, the LF component of the current (obtained by averaging over the RF period) is also presented (in black). (b) Temporal evolution of the voltage recorded over the top (LF-powered, in blue) and bottom (RF-powered, in black) electrodes (with the same ground). Here, the LF and RF voltage amplitudes are set to 650 and 195 V, respectively. Of note, the polarity of the RF signal was inverted with respect to the one measured to account for the fact that both voltages are not measured on the same electrode of the DBD cell. The small RF 5MHz component on the measured LF voltage is not applied on LF electrode but is rather an artefact (parasitic voltage picked up by the probe). As expected, small RF modulations are observed in the LF component due to the corresponding rise in current calling for an enhanced power input [41]. *Small variations of the applied RF voltage are also seen throughout the LF cycle, as explained in* [14].

3.2 Optical diagnostics of α – γ DF-DBDs

As described in previous studies [14], the main optical signals observed during optical emission spectroscopy of Ar-NH_3 DF-DBDs are continuum emission between 300 and 650 nm attributed to the electron-neutral bremsstrahlung [19], [29] and Ar lines between 650 and 950 nm linked to Ar $2p_x \rightarrow 1s_y$ transitions [42]. On one hand, in weakly-ionized RF plasmas, for a fixed population of neutral gas atoms, the behavior of the continuum emission intensity can be related to the electron number density and to the average electron energy (or electron temperature, assuming Maxwellian energy distribution function) [19], [43]. On the other hand, in the specific case of the 750.4 nm line (Ar $2p_1 \rightarrow 1s_2$), assuming that the emitting Ar $2p_1$ state is mostly populated by electron-impact excitation from ground-state Ar atoms (this process requires an energy of 13.48 eV) [44], it can be assumed that this line emission intensity characterizes the presence of high-energy electrons [45]–[47]. Figure 2 (a) and Figure 2 (b) present the spatio-temporal evolution of the emission intensities of the continuum at 500 nm (to avoid overlap with Ar $2p_x \rightarrow 1s_y$ transitions) and of 750.4 nm (Ar $2p_1 \rightarrow 1s_2$) argon line, both recorded in the same experimental conditions as in Figure 1. Here, in a region focused around the LF positive current peak (Figure 1 (a)), between 0.5 and 3 µs, the LF cathode is the upper electrode.

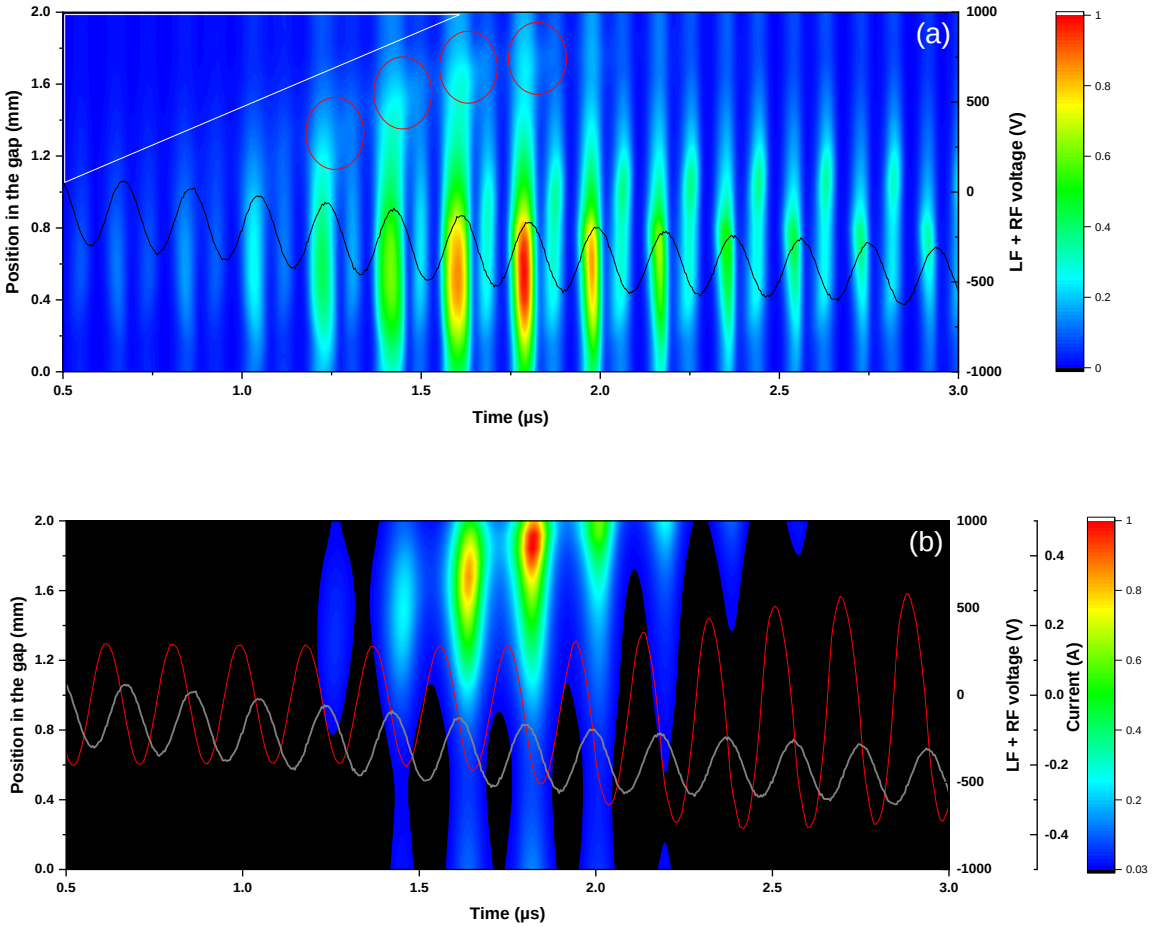

Figure 2. Normalized spatio-temporal mapping of (a) the Bremsstrahlung continuum emission (500 nm) and (b) the Ar $2p_1 \rightarrow 1s_2$ (750.4 nm) line emission intensity recorded in the inter-electrode gap during γ breakdown of the LF-RF DBD produced at 650 V LF voltage and 195 V RF voltage. The upper electrode is the LF cathode. See text for details on highlighted regions. Here, the red sinusoidal waveform on (b) is the current and the grey one corresponds to the addition of the LF and RF voltage presented in Figure 1 (after removal of the parasitic RF component on the LF signal) whixh is the voltage applies between the electrodes.

In Figure 2 (a), a triangular zone with very weak continuum emission is observed in the top left corner (represented by a white triangle). Such weak emission can be attributed to the reduced electron number density in the cathode sheath, which contrasts with the high electron densities seen in this region during γ breakdown (between 1.25 and 2.25 µs) [14]. Here, the sheath position was only roughly identified as the

intensity of the continuum emission is linked to both electron temperature and density [19], [43]. Hence, even if the electron density sharply decreases in the sheath, the rise in electron temperature could lead to some bremsstrahlung emission, which renders difficult a clear identification of the boundary between the sheath and the bulk. Figure 2 (a) further reveals that between 1.2 and 1.8 µs, continuum emission of the two alternances of the RF appear to be joined in the sheath edge zone (see red circles in Figure 2 (a)); however, they are disjointed elsewhere, including at the same position in the gap between the negative and positive RF half cycles. Notably, the junction approaches the cathode with time throughout the LF cycle; this phenomenon is linked to the contraction of the LF sheath in the γ mode (additional details are provided below). In the bulk, the continuum emission appears twice per RF period, and its amplitude and position depend on the RF polarity. More specifically, maximum intensity is always achieved when a negative RF voltage is applied to the upper electrode (*i.e.,* same as the LF cathode). In terms of position, when the upper electrode is LF cathode with negative RF applied voltage, the maximum is strongly shifted from the middle of the gap towards the LF anode. On the other hand, when the upper electrode is LF cathode with positive RF applied voltage, the maximum occurs closer to the middle of the gap. Considering that the continuum emission is mostly observed in conditions characterized by high electron populations [14], therefore, in the RF plasma bulk, the shift towards the LF anode when the upper electrode is the cathode for both RF and LF signifies a displacement of the plasma bulk along that direction due to the corresponding time evolution of the LF cathode sheath.

In α – γ DF-DBDs, γ breakdown is initiated when the voltage applied to the gas reaches a maximum such that the electric field in the sheath is nearly maximum and electrons become strongly accelerated in this region [14]. In line with the prominent excitation pathway of the Ar($2p_1$) state, the 750.4 nm line emission intensity presented in Figure 2 (b) reveals a drastic increase in the cathode sheath linked to the presence of a significant population of high-energy electrons in this region. Figure 2 (b) further shows that, as the

sheath contracts during the α–to-γ mode transition, the maximum emission progressively approaches the cathode. Notably, maximum 750.4 nm emission is reached at about 0.6 µs before the maximum in current (Figure 1 (a)) due to the drastic decrease in gas voltage during γ discharge development, as in the case of a low frequency DBD [14]. Compared to the maximum of the continuum emission (Figure 2 (a)), the maximum of the 750.4 nm emission (Figure 2 (b)) is delayed by about 30 ns. Such difference in time between the two maxima can be explained by the lifetime of $Ar(2p_1)$ state (22 ns) which would delay 750.4 nm photon emission. Beyond its maximum intensity in the half-cycle of the applied LF voltage (~1.8 µs), Figure 2 (b) reveals that the 750.4 nm line emission intensity decreases due to the progressive extinction of the γ mode (linked to the charging of the dielectrics, the rise in the voltage across the dielectrics, and thus the corresponding decrease in the gas voltage [14]).

During a RF cycle, it can be seen in Figure 2 (b) that the 750.4 nm emission is maximum shortly after the RF and LF polarities are the same. However, during the γ mode (around 1.4 to 2.3 µs) the emission is always observed near the LF cathode, regardless of RF polarity, but not on the LF anode side. When the emission is highest at the cathode, that is, when the polarities of the two voltages are the same, the discharge crosses the gap and reaches the anode (once every RF cycle). This can be explained by the drift of electrons created in the sheath towards the anode. When the RF applied voltage is negative at the lower electrode, then the 750.4 nm emission is no longer measured in the lower half part of the gap, close to the LF anode. Therefore, there is a difference between the 750.4 nm emission at the LF cathode and the LF anode: near the cathode, the line emission intensity remains high regardless of the RF polarity, but at the anode, the emission is only observed when this electrode is also the powered by a positive RF applied voltage.

4. Fluid modeling and discussion

4.1 α – γ DF-DBDs

Overall, the emission intensities of the continuum and Ar 750.4 nm line, presented in Figure 2 (a) and (b), reveal that the total electron number density and the population of high-energy electrons strongly depend on the position of the plasma bulk relative to the LF sheath. Although different trends are observed for the two optical signals, the behaviors are always related to the polarities of the RF and LF voltages, and thus to dual-frequency sheath oscillations. The aim of this part is to explain the relationship between sheath oscillations, emission intensity and current dissymmetry. In this context, the spatio-temporal evolution of the electron source term, electric field, electron and ion fluxes are analyzed using a 1D fluid model of Ar-based DBDs developed and validated in a previous work [30]. Note that this model solves the continuity and momentum equations for all species and the energy equation for electrons. It considers 7 species (Ar, Ar^+, Ar_2^+, Ar(1s), Ar_2*, photons and e^-) through 11 reactions. Secondary electron emission from dielectric surfaces, induced by impinging of Ar^+, Ar_2^+, Ar(1s), Ar_2* and VUV photons, is also considered. Hence, this model does not account for NH_3 dissociation (and the presence of reaction products such as NH, NH_2, N_2, and H_2 in the gas phase [48]). In addition, the value for the RF frequency selected in the simulations (5 MHz) is slightly less than the one used in the experiments (5.3 MHz); as shown below, this explains why the time interval during which the DBD is in the γ mode obtained from the model do not exactly coincide with the one seen in the experiments.

Figure 3 depicts the spatio-temporal distribution of the source term in the electron particle balance equation (in $m^{-3}.s^{-1}$) deduced from the model (see details in [23]) in the case wherein the LF cathode is the top electrode and the RF voltage oscillates. Of note, in line with the 750.4 nm emission, this source term can be linked with the population of high-energy electrons [30]. In general, Figure 3 indicates that electrons

are mainly produced near the LF cathode, where the continuum emission is low and the 750.4 nm emission is high. Although, in this zone, the electron number density seems to be small (Figure 2 (a)), their average energy is high (Figure 2 (b)), which is consistent with the properties of a cathode sheath. Indeed, the electrons created in the sheath are subjected to a strong electric field, which induces their rapid acceleration towards the bulk. After the γ breakdown, the maximum of the electron source term moves closer to the cathode due to the contraction of the LF sheath. In line with the behavior of 750.4 nm emission presented in Figure 2 (b), the electron source is high at the LF cathode regardless of the RF polarity, whereas at the anode, it is significant only once per RF cycle.

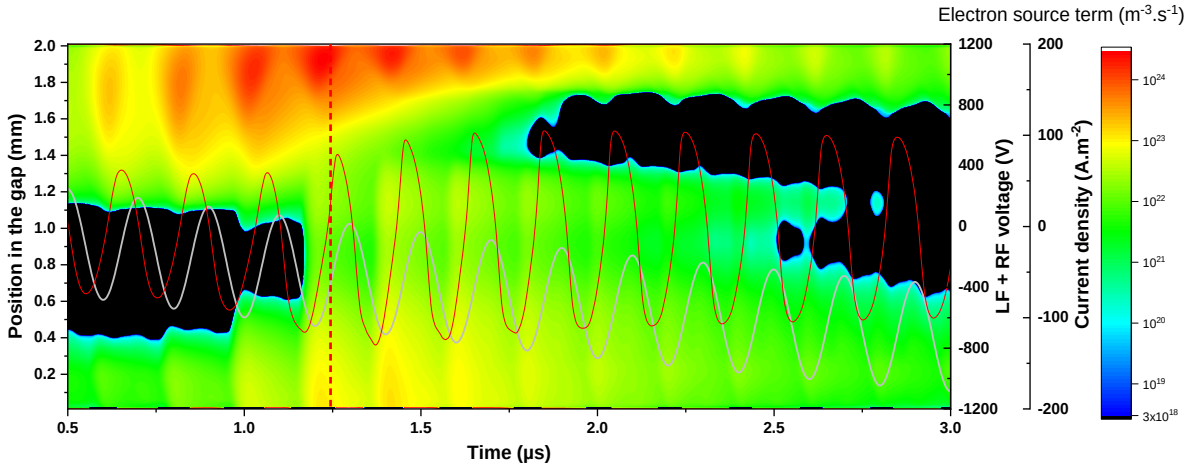

Figure 3. Spatio-temporal distribution of the source term in the electron particle balance equation obtained from the model. The black regions signify negative values or below the threshold of 3.10^{18} $m^{-3}s^{-1}$. The results are shown during γ breakdown of a LF-RF DBD produced at 940 V LF voltage and 350 V RF voltage. Of note, the LF and RF voltage amplitudes used in the model are slightly different from those used in the experiments; additional details are provided in [14]. *Voltage and current density are presented respectively in grey and red. The upper electrode is the LF cathode. The red dashed line, from Figure 3 to Figure 6, illustrates one of the times for which V_{RF}=0*

The spatio-temporal mapping of the electric field is shown in Figure 4, wherein positive and negative values are presented in red and blue, respectively, and the solid black line represents 0 electric field. When the electric field is positive, the electrons drift towards the bottom electrode (the LF anode), whereas the ions

drift towards the upper electrode (the LF cathode). This trend is reversed when the electric field is negative. Considering that a high positive electric field (corresponding to the cathode sheath) is always present at the upper electrode (recall that the amplitude of the LF voltage is higher than the one of the RF voltage), the electrons created in the sheath always drift to the plasma bulk, and their density is thus rather low in the sheath. Between 0.5 and 1.5 µs, the high electric field zone near the upper electrode contracts due to the ion density increase related to the sudden production of electrons and ions during γ breakdown, and the rapid transport of electrons towards the gas bulk; this is consistent with the contraction of the sheath. In the bulk, the electric field alternates between positive and negative values, according to the RF voltage polarity. When it is positive, the electrons in the gas bulk drift toward the LF anode. However, when it is negative, both, the electrons in the sheath and those in the bulk are accelerated towards the sheath edge. Therefore, the negative electric field achieved in the bulk at opposite RF and LF polarities leads to electron trapping at the sheath edge of the LF cathode sheath. Such trapping results in high electron number density on a local scale (see Figure 5 (b)), especially considering that the trapped electrons cannot escape to the cathode via diffusion. When the polarities of the RF and LF voltages are the same, the accumulated electrons are evacuated towards the LF anode.

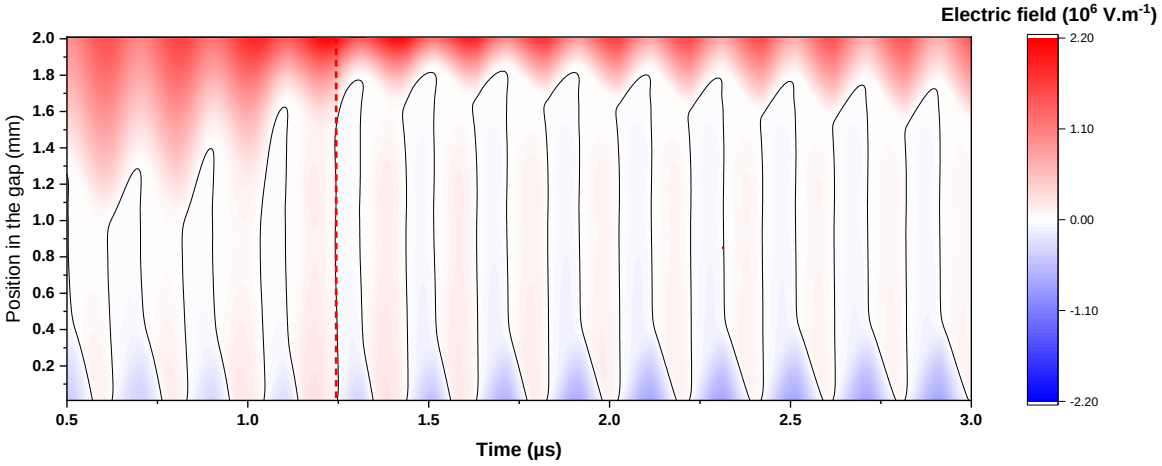

Figure 4. Spatio-temporal distribution of the electric field (positive in red, negative in blue). The simulation conditions are the same as in Figure 3.

The spatio-temporal distribution of the number density of charged species and electron temperature in the α – γ DF-DBDs are presented in Figure 5. In Figure 5 (a), the density of ions is maximum at the cathode during γ breakdown, at around 1.5 µs, as in [14]. At this time, a cathode sheath is present (see Figure 4). The density of ions is also quite high in the bulk center. Notably, the ion density is relatively stable at tens of ns time scale: as expected, despite the electric field oscillations, the ions are only slightly mobile at the RF scale. To examine the spatio-temporal evolution of the cathode sheath length, the mapping of the electron number density in space and time is also analyzed. In Figure 5 (b), the sheath, at LF and RF scales, can be defined by the blue zone corresponding to a low electron number density region. Clearly, the RF oscillations modifies the sheath length on both the LF cathode (top electrode) and the LF anode (bottom electrode). However, the LF cathode sheath oscillates but remains present, regardless of the polarity of the RF voltage while, at the LF anode, the sheath disappears when the bottom electrode is powered by a positive RF applied voltage. The same thing can be seen with the high electron temperature zone in Figure 5 (c).

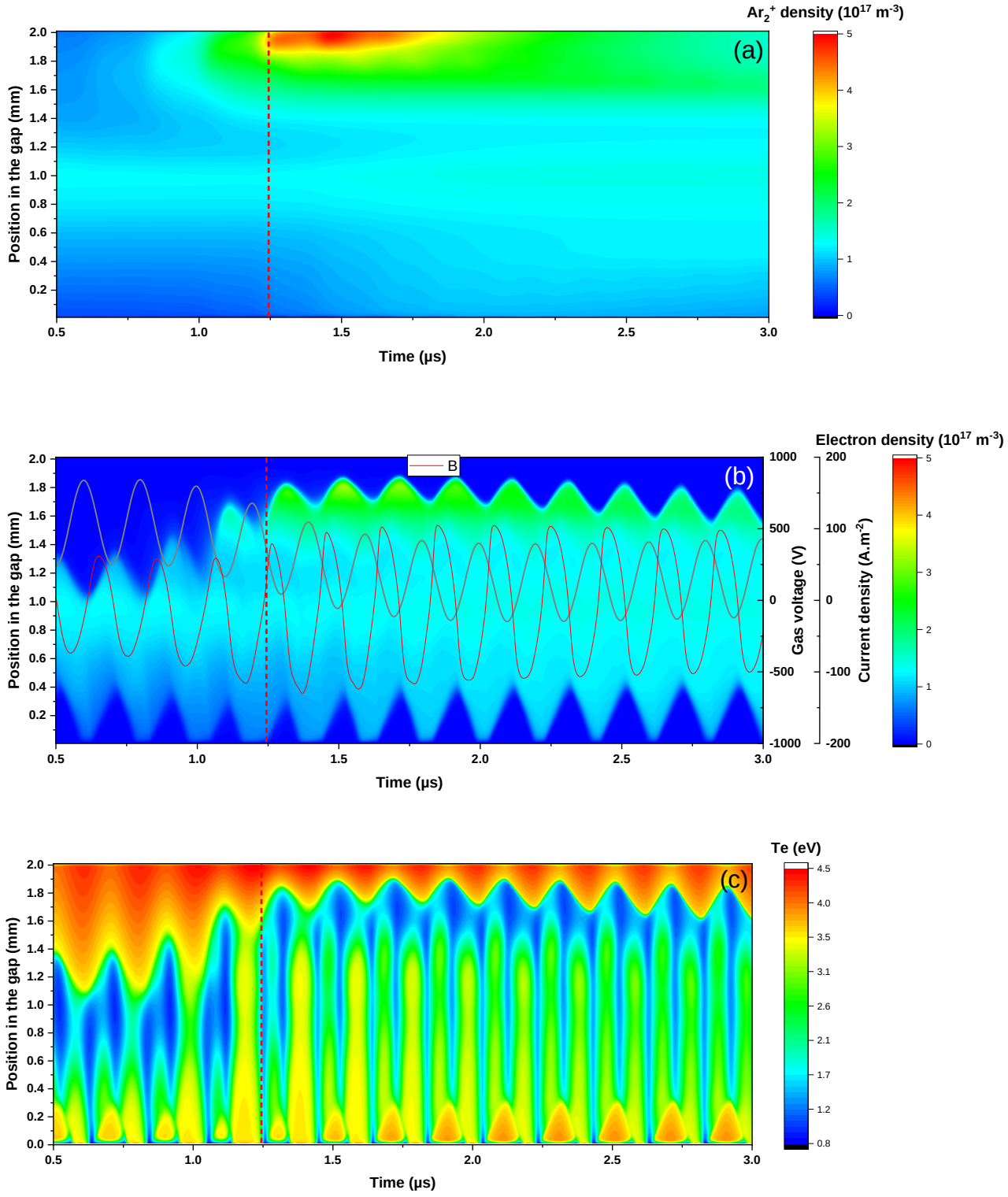

Figure 5. Spatio-temporal distribution of (a) the Ar_2^+ density, (b) the electron number density obtained from the model and (c) the electron temperature. In (b), the gas voltage (in black) and current density (in red) are also shown. The simulation conditions are the same as in Figure 3.

Between 0.6 and 1.5 µs, Figure 5 (b) further shows that the LF cathode sheath (top electrode) contracts, thereby increasing the plasma bulk length. This agrees well with the spatio-temporal mapping of the continuum emission displayed in Figure 2 (a). However, the zone of high electron number density does never reach the upper electrode (LF cathode). In contrast, at the LF anode (bottom electrode), the electrons only reach the anode when the RF and LF voltage polarities are the same. When the RF and LF voltage polarities are opposite, the RF sheath is thinner and shorter in the γ mode than in the α mode. Hence, in such conditions, the electrons reach the LF anode for a longer time in γ mode than in α mode, in agreement with the continuum emission displayed in Figure 2 (a). At the LF cathode sheath edge, it can also be seen in Figure 5 (b) that the maximum electron number density appears once per RF period. Specifically, it occurs when the LF cathode sheath is the shortest, *i.e.*, when the polarities of the two applied voltages are opposite inducing the electron accumulation at the sheath border (see the behavior of the gas voltage, white line in Figure 5 (b)). Such trend is observed between 1.3 and 2.1 µs; however, the maximum production is attained at 1.2 µs. This difference indicates that the electron number density is more related to their transport along the electric field rather than to their precise creation zone in the α – γ DF-DBDs.

The electric field distribution presented in Figure 4 can be attributed to variations of applied voltages and of ion and electron number density distributions (space charge electric field). When γ breakdown occurs, ions and electrons are mostly created in the sheath. Considering that the ion source term is strong in the sheath (whatever its length), when the sheath contracts due to the variation in gas voltage, some ions created when the sheath was the longest, will end up in the bulk, near the sheath edge, locally increasing the ion population. To understand the variation of the electric field sign in the bulk, it is necessary to look

at the ion density and the electron source term in the sheath, at the time scale of the RF cycle. When the electron source term is the highest in the sheath, the number of electrons created becomes very high. To maintain quasi-neutrality in the bulk, the electric field is deformed to evacuate electrons towards the LF anode. In contrast, when the electron source term is low in the sheath, the number of electrons created is too low to neutralize the high ion density at the sheath edge. As a result, the electric field of the bulk must change sign to restore neutrality by transporting electrons from the bulk and the sheath.

Since the current depends on the total flux of charged species at the walls, the fluxes of electrons and ions at the LF cathode (upper electrode, Figure 6 (a)) and of electrons in the whole gap (Figure 6 (b)) were also analyzed. As shown in Figure 6 (a), the electron and ion fluxes at the cathode are strictly negative and positive, respectively, and they are not significantly affected within the RF time scale to be reduced to 0. Close to the LF cathode, ions flow towards the dielectric, whereas the electrons (secondary electrons emitted from the dielectric by impinging ions and VUV photons [30]) migrate towards the plasma bulk. Notably, significant secondary electron emission is detected between 0.6 and 2 µs, with a significant rise during sheath contraction. Meanwhile, the maximum in the ion flux occurs later in the LF cycle and lasts much longer. The variation between the time intervals of the electron and ion fluxes is attributed to the substantial contribution of VUV photons from the plasma to secondary electron production (about 95 % calculated from the model, averaged on a LF period) [30]. Indeed, when γ breakdown occurs and the sheath becomes self-sustained, ions and excited Ar and Ar_2 species are produced in the sheath through collisions with high-energy electrons. The average time for (i) the creation of excited Ar_2^* excimer through conversion of atoms in Ar(1s) states by 3-body collisions with 2 ground state Ar atoms, (ii) the de-excitation of Ar_2^* by VUV photon emission, and (iii) the transport of VUV photons towards the wall to induce secondary electron emission, is much shorter than the time it takes for an ion created in the sheath to

reach the wall. Thus, due to the contribution of VUV photons in the creation of secondary electrons, the secondary electron flux increases faster than the ion flux arriving at the wall [30].

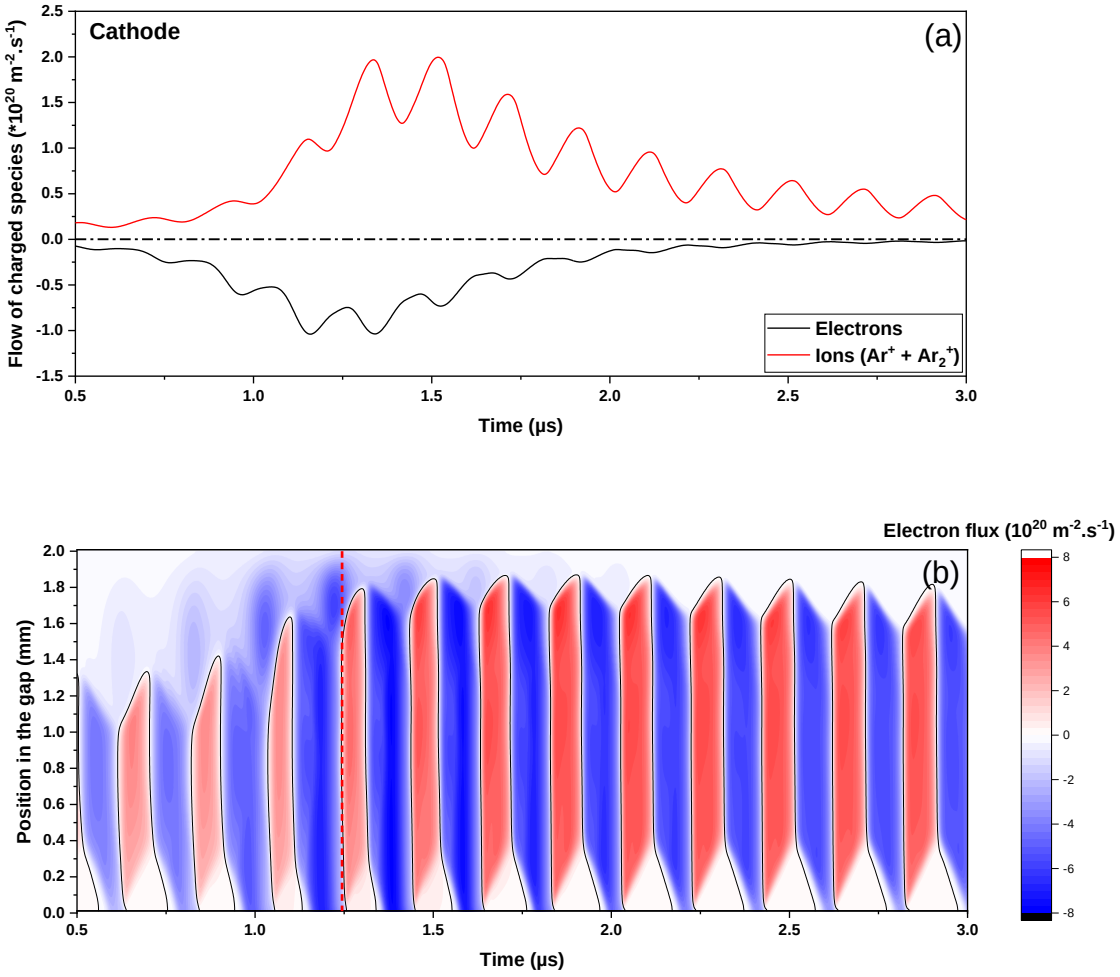

Figure 6. (a) Temporal evolution of the calculated electron and ions fluxes at the LF cathode. (b) Spatio-temporal distribution of the electron flux. A positive flux (in red) is due to electrons moving toward the LF cathode, upper electrode. The white areas depict very small electron flux, and the black line represents the zero values. The simulation conditions are the same as in Figure 3.

In the bulk, Figure 6 (b) shows that the electron flux is alternatively positive, in red, and negative, in blue. On the other hand, near the upper electrode (the LF cathode), it remains negative. Hence, it is controlled by the RF polarity in the gap and by the LF polarity in the LF cathode sheath. The triangular shape discerned at the extremities of positive fluxes at the sheath edge is attributed to its expansion/contraction. This explains the junction of the continuum emission observed in this area in Figure 2. Of note, this junction on the bremsstrahlung continuum emission is related to the contraction of the cathode sheath when polarities of the LF and RF voltages are opposite. This contraction is observed when the high electron negative flux coming from the cathode meets the positive one coming from the bulk. Therefore, the continuum emission is attributed to the high electron populations created from the negative electron flux emanating from the sheath, as well as from the positive electron flux coming from the LF anode to the bulk (this creates a junction in the transition between these two fluxes). Comparatively, when the electron flux is monotonous along the gap, i.e. when polarities of the LF and RF voltages are of the same sign, electrons originating from the sheath are simply dragged towards the anode, decreasing the electron density at the sheath edge. In this configuration, no junction is observed in Figure 2. Furthermore, Figure 6 (b) reveals that during the LF sheath contraction (between 1.13 and 1.25 µs), the negative electron flux at the LF anode lasts longer than anywhere else. At this time, the electron number density at the sheath edge is the highest (see Figure 5 (b)), as electrons cannot be evacuated at the LF cathode. Hence, the electric field is deformed for a longer time to evacuate the electrons towards the anode (see Figure 4).

It is worth highlighting that the behaviors of the electric field seen in Figure 4 and particle flux at the walls shown in Figure 6 can be used to explain the asymmetry between the positive and negative current components reported in Figure 1. As underlined above, and further highlighted in Figure 7, this asymmetry is particularly significant in the 0.5–3 µs time interval, with the positive current component being consistently higher than the negative component (the exact opposite trend is observed during the second

γ breakdown in the other LF half-cycle), and it is detected before and during the γ avalanche period (*i.e.*, as soon as the LF sheath is formed). The strong increase in the current amplitude from 1.25 to 2.5 µs emphasizes the asymmetry. The difference between positive and negative current components during the breakdown is due to the variations in applied voltage and space charge electric field. Because of γ breakdown, strong ionization occurs in the sheath and this causes a strong ion flux to the cathode and an important electron flux to the anode once per RF period [23]. Electrons are accelerated in the LF cathode sheath regardless of the RF polarity, then the electric field in the bulk will accelerate electrons depending on the RF polarity. When the electric field in the bulk is of the same sign as the one in the LF sheath (electrons go towards the anode), the current is the highest (the positive current in Figure 7), but when it is the other way around, the electric field in the bulk and in the sheath are opposite. In this case, mean electron velocities are lower than in the previous case such that the absolute values of the current are also lower.

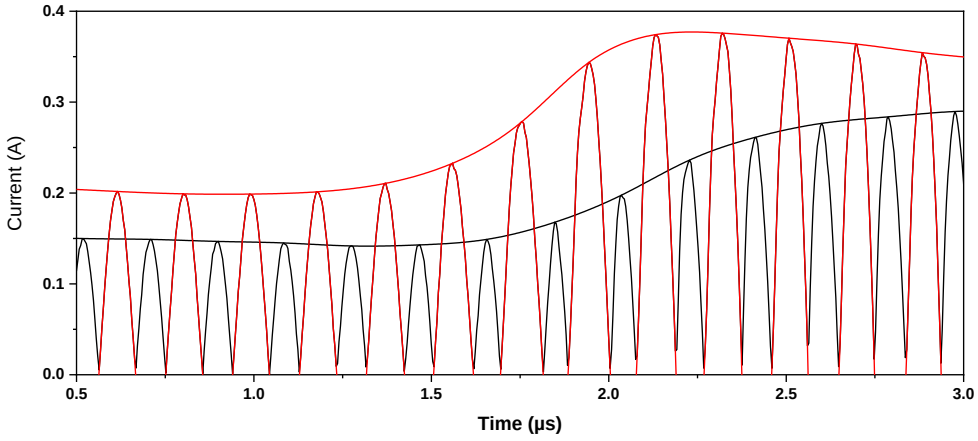

Figure 7. Absolute value of the measured dual frequency current components (positive in red and absolute value of negative in black) and their respective envelopes between 0.5 and 3 µs for LF and RF voltage amplitudes of 650 and 195 V, respectively.

4.2 α DF-DBDs

The asymmetry observed in Figure 7 for DF-DBDs exhibiting the $\alpha - \gamma$ transition is attributed to the production of strong fluxes of charged particles during relatively short periods of time. When the DF-DBD does not allow switching to γ mode (*i.e.*, remaining in RF-α discharge), different results are obtained, as evidenced by the 1D fluid modeling data presented in Figure 8. Here, the α discharge regime is maintained by using a lower amplitude of the applied LF voltage (LF 400 V in Figure 8, instead of LF 940 V in Figure 3 to Figure 6; additional details can be found in [23]). For LF 400 V, there is no self-sustainment in the cathode sheath, which results in a low creation rate of electrons and ions in the sheath. Consequently, as shown in Figure 8, the electron and ion densities are highest in the bulk, as in the case of RF α discharges [49].

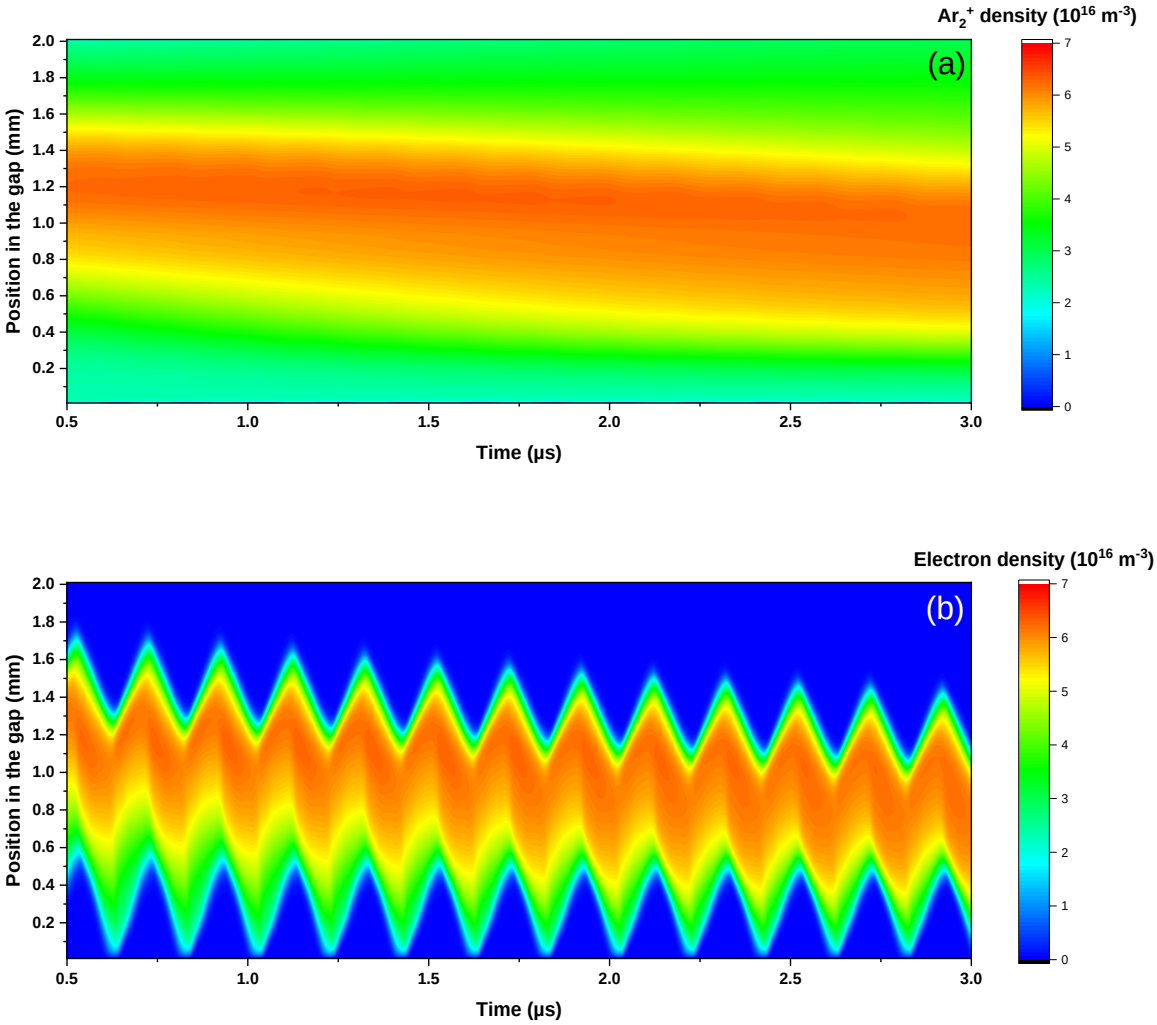

Figure 8. Spatio-temporal distribution of the calculated Ar_2^+ ion density (a) and electron number density (b) running in RF-a mode. The results are shown between 0.5 and 3 μs for LF and RF voltage amplitudes of 400 and 350 V, respectively.

Figure 8 further shows that the ion and electron densities corresponding to the α mode do not present a maximum in the sheath or at the sheath edge. Indeed, both densities are minimum in the sheath, resulting in little sheath contraction and no strong flux to the wall. Therefore, the dielectric voltage does not change suddenly, and the gas and applied voltages remain almost the same (Figure 9 (a)). In this case, the (RF-averaged) sheath lengths changes gradually over the LF period, as seen in the ion and electron number

density distributions. Moreover, as depicted in Figure 9 (b), very little asymmetry in the current density is detected for the α DF-DBDs.

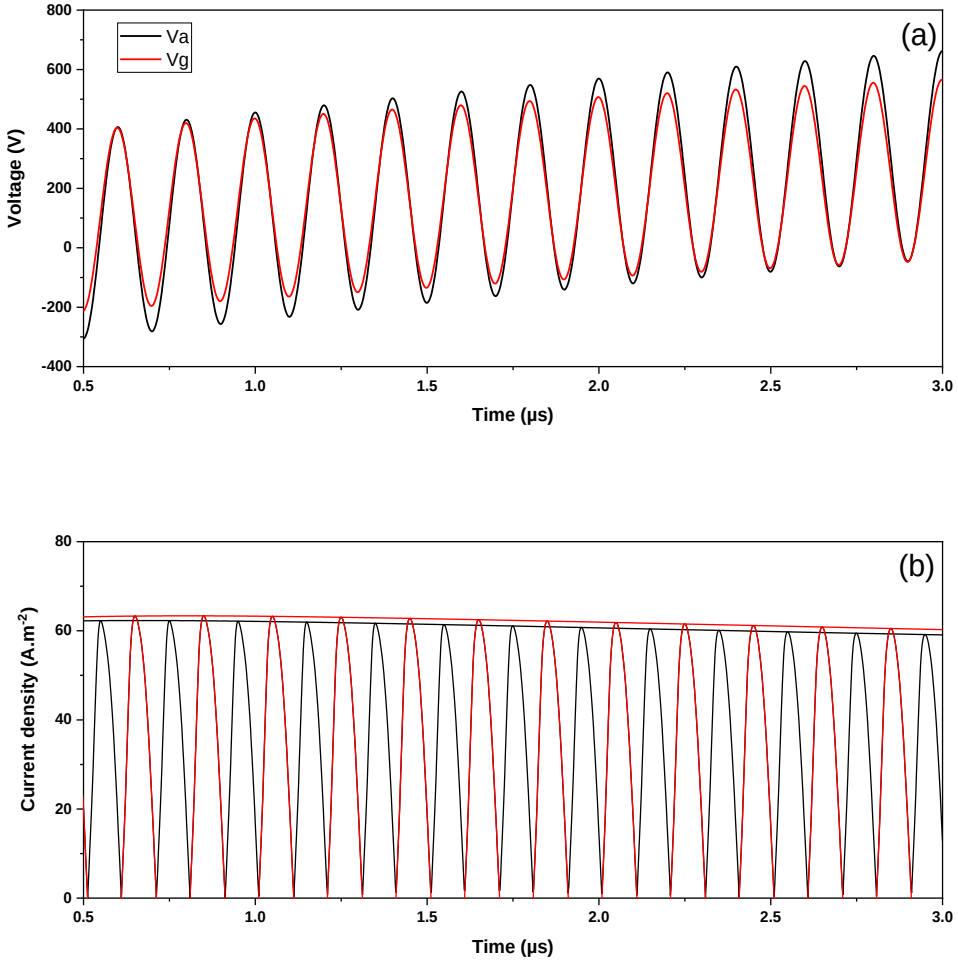

Figure 9. (a) Temporal evolution of the applied voltage (in black) and gas voltage (in red). (b) Current density components (positive in red and negative (absolute value) in black) and their respective envelopes. The results are shown between 0.5 and 3 µs for LF and RF voltage amplitudes of 400 and 350 V, respectively.

5. Conclusion

This article is focused on the γ mode of a DF-DBD, where the effect of the dual-frequency sheath oscillations is the most important and thus the most visible. It was observed that the presence of a LF sheath influences the functioning of the DF-DBD whatever the discharge mode, as long as a LF component on the applied voltage is present. The set of electrical and optical measurements reported in this work reveals two different behaviors. First, when the polarities of the LF and RF voltages are opposite, an electric field drives the electrons near the LF cathode sheath towards the plasma bulk and an opposite electric field present from the sheath edge to the LF anode pushes the electrons towards the LF cathode sheath. In such conditions, in the LF cathode sheath, the only modification is the amplitude of the electric field, and the sheath length. However, at the LF sheath edge, electrons become trapped and ions drift towards the cathode and the anode simultaneously according to their position in the gap. A second behavior appears when the RF voltage has the same polarity as the LF voltage. In this case, the electric field along the gap exhibits the same polarity as the one in the sheath, allowing electrons created in the sheath to be evacuated towards the LF anode. The behavior of the LF cathode is therefore controlled by the LF sheath, and thus by the LF voltage, while the one in the bulk and at the anode alternates on the time scale of the RF voltage. This analysis explains the asymmetry between the positive and negative current at the RF scale observed during the γ mode of the DF-DFDs.

6. Acknowledgments

The work carried out in France was supported by the Agence Nationale de la Recherche through the Investissement d'avenir program (ANR10LABX2201). As for the one done in Canada, it was funded by the Natural Sciences and Engineering Research Council of Canada (NSERC RGPIN-2018-04550) and by the Fondation Courtois. The 'Réseau des Plasmas Froids' of CNRS/MCRT (France) is acknowledged for providing

the DFB diode laser and the travel support for Nader Sadeghi, and LPGP in Orsay (France) for lending the MCS6A Multiscaler. All authors would like to acknowledge the financial support of the CNRS and Université de Montréal through their contributions to the International Research Network on Controlled Multifunctional Nanomaterials (IRN NMC).

7. Data availability statement

The data that support the findings of this study are available from the corresponding author upon reasonable request.

8. References

[1] R. Bartnikas, "Note on ac discharges between metallic-dielectric electrodes in helium," *J. Appl. Phys.*, vol. 40, no. 4, pp. 1974–1976, 1969.

[2] S. Kanazawa, M. Kogoma, T. Moriwaki, and S. Okazaki, "Stable glow plasma at atmospheric pressure," *J. Phys. D. Appl. Phys.*, vol. 21, no. 5, pp. 838–840, 1988.

[3] S. Kanazawa, M. Kogoma, S. Okazaki, and T. Moriwaki, "Glow plasma treatment at atmospheric pressure for surface modification and film deposition," *Nucl. Inst. Methods Phys. Res. B*, vol. 37–38, no. C, pp. 842–845, 1989.

[4] C. Liu and J. R. Roth, "Plasma-related characteristics of a steady state glow discharge at atmospheric pressure," vol. 00226020, no. 3, pp. 1–8, 1993.

[5] F. Massines, A. Rabehi, P. Decomps, R. Ben Gadri, P. Ségur, and C. Mayoux, "Experimental and theoretical study of a glow discharge at atmospheric pressure controlled by dielectric barrier," *J. Appl. Phys.*, vol. 83, no. 6, pp. 2950–2957, 1998.

[6] C. Tyl *et al.*, "Investigation of memory effect in atmospheric pressure dielectric barrier discharge in nitrogen with small oxygen or nitric oxide addition," *J. Phys. D. Appl. Phys.*, vol. 51, no. 35, p. 354001, 2018.

[7] X. Lin, C. Tyl, N. Naudé, N. Gherardi, N. A. Popov, and S. Dap, "The role of associative ionization reactions in the memory effect of atmospheric pressure Townsend discharges in N2 with a small O2 addition," *J. Phys. D. Appl. Phys.*, vol. 53, no. 20, p. 205201, 2020.

[8] C. Douat, I. Kacem, N. Sadeghi, G. Bauville, M. Fleury, and V. Puech, "Space-time resolved density of helium metastable atoms in a nanosecond pulsed plasma jet: Influence of high voltage and pulse frequency," *J. Phys. D. Appl. Phys.*, vol. 49, no. 28, p. 285204, 2016.

[9] F. Massines, N. Gherardi, N. Naudé, and P. Ségur, “Recent advances in the understanding of homogeneous dielectric barrier discharges,” *EPJ Appl. Phys.*, vol. 47, no. 2, p. 22805, 2009.

[10] R. Bazinette, R. Subileau, J. Paillol, and F. Massines, “Identification of the different diffuse dielectric barrier discharges obtained between 50kHz to 9MHz in Ar/NH3 at atmospheric pressure,” *Plasma Sources Sci. Technol.*, vol. 23, no. 3, p. 035008, 2014.

[11] M. Moravej, X. Yang, M. Barankin, J. Penelon, S. E. Babayan, and R. F. Hicks, “Properties of an atmospheric pressure radio-frequency argon and nitrogen plasma,” *Plasma Sources Sci. Technol.*, vol. 15, no. 2, pp. 204–210, 2006.

[12] R. Bazinette, J. F. Lelièvre, L. Gaudy, and F. Massines, “Influence of the Discharge Mode on the Optical and Passivation Properties of SiNx:H Deposited by PECVD at Atmospheric Pressure,” *Energy Procedia*, vol. 92, pp. 309–316, 2016.

[13] J. S. Boisvert, L. Stafford, N. Naudé, J. Margot, and F. Massines, “Electron density and temperature in an atmospheric-pressure helium diffuse dielectric barrier discharge from kHz to MHz,” *Plasma Sources Sci. Technol.*, vol. 27, no. 3, p. 035005, 2018.

[14] R. Robert, G. Hagelaar, N. Sadeghi, L. Stafford, and F. Massines, “Influence of the RF voltage amplitude on the space- and time-resolved properties of RF-LF dielectric barrier discharges in α–γ mode,” *Work Submitt. Publ.*

[15] V. A. Godyak and R. B. Piejak, “Abnormally low electron energy and heating-mode transition in a low-pressure argon rf discharge at 13.56 MHz,” *Phys. Rev. Lett.*, vol. 65, no. 8, pp. 996–999, 1990.

[16] J. S. Boisvert, J. Margot, and F. Massines, “Transitions between various diffuse discharge modes in atmospheric-pressure helium in the medium-frequency range,” *J. Phys. D. Appl. Phys.*, vol. 49, no. 32, p. 325201, 2016.

[17] M. M. Turner and P. Chabert, “Electron heating mode transitions in dual frequency capacitive discharges,” *Appl. Phys. Lett.*, vol. 89, no. 23, pp. 9–11, 2006.

[18] Y. Liu, S. A. Starostin, F. J. J. Peeters, M. C. M. Van De Sanden, and H. W. De Vries, “Atmospheric-pressure diffuse dielectric barrier discharges in Ar/O2 gas mixture using 200 kHz/13.56 MHz dual frequency excitation,” *J. Phys. D. Appl. Phys.*, vol. 51, no. 11, p. 114002, 2018.

[19] R. Magnan, G. Hagelaar, M. Chaker, and F. Massines, “Atmospheric pressure dual RF – LF frequency discharge : transition from α to α–γ -mode,” *Plasma Sources Sci. Technol.*, vol. 30, no. 1, p. 015010, Jan. 2021.

[20] F. Massines, R. Bazinette, and J. Paillol, “RF-LF dual frequency uniform dielectric barrier discharge for thin film processing,” *22nd Int. Symp. Plasma Chem.*, p. O-22-3, 2015.

[21] D. Liu, A. Yang, X. Wang, C. Chen, M. Rong, and M. G. Kong, “Electron heating and particle fluxes in dual frequency atmospheric-pressure helium capacitive discharge,” *J. Phys. D. Appl. Phys.*, vol. 49, no. 49, pp. 1–7, 2016.

[22] J. Waskoenig and T. Gans, “Nonlinear frequency coupling in dual radio-frequency driven atmospheric pressure plasmas,” *Appl. Phys. Lett.*, vol. 96, no. 18, pp. 3–6, 2010.

[23] R. Magnan, G. Hagelaar, M. Chaker, and F. Massines, “Atmospheric pressure dual RF-LF frequency discharge: Influence of LF voltage amplitude on the RF discharge behavior,” *Plasma Sources Sci. Technol.*, vol. 29, no. 3, p. 035009, Feb. 2020.

[24] J. J. Shi and M. G. Kong, “Mode transition in radio-frequency atmospheric argon discharges with and without dielectric barriers,” *Appl. Phys. Lett.*, vol. 90, no. 10, p. 101502, 2007.

[25] D. W. Liu, F. Iza, and M. G. Kong, “Electron heating in radio-frequency capacitively coupled atmospheric-pressure plasmas,” *Appl. Phys. Lett.*, vol. 93, no. 26, pp. 1–4, 2008.

[26] Y. J. Zhou, Q. H. Yuan, F. Li, X. M. Wang, G. Q. Yin, and C. Z. Dong, “Nonequilibrium atmospheric pressure plasma jet using a combination of 50 kHz/2 MHz dual-frequency power sources,” *Phys. Plasmas*, vol. 20, no. 11, p. 113502, 2013.

[27] Y. Sun, Z. Zhang, and J. W. M. Lim, “Enhancement of discharge properties of atmospheric pressure plasma systems through trace radio-frequency oscillation control,” *Plasma Sources Sci. Technol.*, vol. 30, no. 7, p. 075018, 2021.

[28] R. Bazinette, N. Sadeghi, and F. Massines, “Dual frequency DBD: Influence of the amplitude and the frequency of applied voltages on glow, Townsend and radiofrequency DBDs,” *Plasma Sources Sci. Technol.*, vol. 29, no. 9, p. 095010, 2020.

[29] S. Park, W. Choe, S. Y. Moon, and J. J. Shi, “Electron Information in Single-And Dual-Frequency Capacitive Discharges at Atmospheric Pressure,” *Sci. Rep.*, vol. 8, no. 1, pp. 1–10, 2018.

[30] R. Robert, G. Hagelaar, N. Sadeghi, R. Magnan, L. Stafford, and F. Massines, “Role of excimer formation and induced photoemission on the Ar metastable kinetics in atmospheric pressure Ar-NH3 dielectric barrier discharges,” *Plasma Sources Sci. Technol.*, vol. 31, no. 6, p. 065010, 2022.

[31] Z. L. Zhang, J. W. M. Lim, Q. Y. Nie, X. N. Zhang, and B. H. Jiang, “Electron heating and mode transition in dual frequency atmospheric pressure argon dielectric barrier discharge,” *AIP Adv.*, vol. 7, no. 10, p. 105313, 2017.

[32] C. Oneill, J. Waskoenig, and T. Gans, “Tailoring electron energy distribution functions through energy confinement in dual radio-frequency driven atmospheric pressure plasmas,” *Appl. Phys. Lett.*, vol. 101, no. 15, pp. 1–5, 2012.

[33] D. O’Connell, T. Gans, E. Semmler, and P. Awakowicz, “The role of the relative voltage and phase for frequency coupling in a dual-frequency capacitively coupled plasma,” *Appl. Phys. Lett.*, vol. 93, no. 8, pp. 1–3, 2008.

[34] T. Gans, D. O’Connell, V. Schulz-Von Der Gathen, and J. Waskoenig, “The challenge of revealing and tailoring the dynamics of radio-frequency plasmas,” *Plasma Sources Sci. Technol.*, vol. 19, no. 3, p. 034010, 2010.

[35] D. Ziegler *et al.*, “The influence of the relative phase between the driving voltages on electron heating in asymmetric dual frequency capacitive discharges,” *Plasma Sources Sci. Technol.*, vol. 19, no. 4, p. 045001, 2010.

[36] B. Bruneau, T. Novikova, T. Lafleur, J. P. Booth, and E. V. Johnson, “Ion flux asymmetry in radiofrequency capacitively-coupled plasmas excited by sawtooth-like waveforms,” *Plasma Sources Sci. Technol.*, vol. 23, no. 6, p. 065010, 2014.

[37] B. Bruneau, T. Gans, D. O’Connell, A. Greb, E. V. Johnson, and J. P. Booth, “Strong ionization asymmetry in a geometrically symmetric radio frequency capacitively coupled plasma induced by sawtooth voltage waveforms,” *Phys. Rev. Lett.*, vol. 114, no. 12, pp. 1–5, 2015.

[38] A. V. Pipa, J. Koskulics, R. Brandenburg, and T. Hoder, “The simplest equivalent circuit of a pulsed

dielectric barrier discharge and the determination of the gas gap charge transfer," *Rev. Sci. Instrum.*, vol. 83, no. 11, p. 115112, 2012.

[39] P. Belenguer and J. P. Boeuf, "Transition between different regimes of rf glow discharges," *Phys. Rev. A*, vol. 41, no. 8, pp. 4447–4459, 1990.

[40] I. Y. Baranov, "Low-current moderate-pressure RF discharge with secondary electron photoemission," *Plasma Phys. Reports*, vol. 28, no. 1, pp. 71–77, 2002.

[41] S. S. Ivković, B. M. Obradović, N. Cvetanović, M. M. Kuraica, and J. Purić, "Measurement of electric field development in dielectric barrier discharge in helium," *J. Phys. D. Appl. Phys.*, vol. 42, no. 22, p. 225206, 2009.

[42] E. Desjardins *et al.*, "Time-resolved study of the electron temperature and number density of argon metastable atoms in argon-based dielectric barrier discharges," *Plasma Sources Sci. Technol.*, vol. 27, no. 1, pp. 1–8, 2018.

[43] R. Bazinette, J. Paillol, and F. Massines, "Optical emission spectroscopy of glow, Townsend-like and radiofrequency DBDs in an Ar/NH3 mixture," *Plasma Sources Sci. Technol.*, vol. 24, no. 5, p. 55021, 2015.

[44] M. Schulze, A. Yanguas-Gil, A. Von Keudell, and P. Awakowicz, "A robust method to measure metastable and resonant state densities from emission spectra in argon and argon-diluted low pressure plasmas," *J. Phys. D. Appl. Phys.*, vol. 41, no. 6, p. 065206, 2008.

[45] J. B. Boffard, G. A. Piech, M. F. Gehrke, L. W. Anderson, and C. C. Lin, "Measurement of electron-impact excitation cross sections out of metastable levels of argon and comparison with ground-state excitation," *Phys. Rev. A - At. Mol. Opt. Phys.*, vol. 59, no. 4, pp. 2749–2763, 1999.

[46] Y. K. Lee, S. Y. Moon, S. J. Oh, and C. W. Chung, "Determination of metastable level densities in a low-pressure inductively coupled argon plasma by the line-ratio method of optical emission spectroscopy," *J. Phys. D. Appl. Phys.*, vol. 44, no. 28, p. 285203, 2011.

[47] G. Nayak, M. Simeni Simeni, J. Rosato, N. Sadeghi, and P. J. Bruggeman, "Characterization of an RF-driven argon plasma at atmospheric pressure using broadband absorption and optical emission spectroscopy," *J. Appl. Phys.*, vol. 128, no. 24, p. 243302, 2020.

[48] R. A. Arakoni, A. N. Bhoj, and M. J. Kushner, "H2 generation in Ar/NH3 microdischarges," *J. Phys. D. Appl. Phys.*, vol. 40, no. 8, pp. 2476–2490, 2007.

[49] N. Balcon, G. J. M. Hagelaar, and J. P. Boeuf, "Numerical model of an argon atmospheric pressure RF discharge," *IEEE Trans. Plasma Sci.*, vol. 36, no. 5 SUPPL. 4, pp. 2782–2787, 2008.